THE JOURNAL OF PHYSICAL CHEMISTRY C

Article

pubs.acs.org/JPCC

Structural Patterns in Carbon Chemisorption on an Icosahedral Iron Cluster

G. L. Gutsev,*[,†] C. A. Weatherford,[†] P. Jena,[‡] E. Johnson,[§] and B. R. Ramachandran[∥]

[†]Department of Physics, Florida A&M University, Tallahassee, Florida 32307, United States

[‡]Department of Physics, Virginia Commonwealth University, Richmond, Virginia 23284, United States

[§]Environmental Sciences Institute, Florida A&M University, Tallahassee, Florida 32307, United States

[∥]College of Engineering & Science, Louisiana Tech University, Ruston, Louisiana 71272, United States

Supporting Information

ABSTRACT: Carbon chemisorption on iron nanoparticles at small carbon coverage has been studied by using a Fe_{13} particle as a model because it possesses a nearly icosahedral geometry, and complications with additional effects associated with the surface inhomogeneity do not arise. The electronic and geometrical structures of $Fe_{13}C_n$ are computed for n = 0−20 using an all-electron density functional theory with generalized gradient approximation and a rather large basis set. It is found that the energetically preferred structures correspond to the formation of carbon dimers up to $Fe_{13}C_{12}$ and trimers up to $Fe_{13}C_{18}$ in octahedral configurations of the dimers and trimers with the Fe_{13} cluster being endohedral. The trend for the formation of carbon tetramers breaks at $Fe_{13}C_{20}$. We found that the dependence of the total energy on the total spin is nearly the same for Fe_{13} and $Fe_{13}C_8$. When the number of chemisorbed carbon atoms exceeds 6, chemisorption quenches the total magnetic moment to 36 μ_B from the value of 44 μ_B in the ground-state Fe_{13} cluster. We used natural atomic orbital populations to understand why the quenching does not depend on the number of chemisorbed atoms. Free C_n species were reoptimized at the same level of theory to calculate the dissociation energies of C_n and $Fe_{13}C_n$. It is found that the largest fragmentation energy of 12 eV belongs to the $Fe_{13}C_{12} \rightarrow Fe_{13} + C_{12}$ channel. Finally, we found that atomization energies for the carbon chemisorbed on the iron particle are larger by approximately 10 eV than atomization energies of the corresponding free carbon particles, which can be related to the catalytic strength of the Fe_{13} particle.

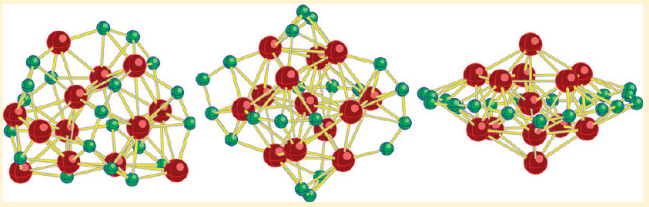

I. INTRODUCTION

Iron particles are widely used for catalyzing the growth of carbon nanotubes (CNTs) using the chemical vapor deposition (CVD)[1] and the high-pressure high-temperature HiPco[2,3] processes. However, despite tremendous experimental and theoretical effort, it is not clear yet how CNTs nucleate on a catalytic iron particle. Theoretical simulations of the CNT growth catalyzed by iron particles have been performed by molecular dynamics methods for the particles composed of 55−1000 iron atoms,[4−7] by an ab initio molecular mechanics method using a Fe_{55} icosahedral particle,[8] by using effective core potentials (ECPs) combined with density functional theory (DFT) methods,[9,10] by using quantum chemical molecular dynamics (QM/MD) methods and iron carbide particles,[11,12] and by using bimetallic particles containing Fe.[13]

In the present work, we use a smaller iron cluster, Fe_{13}, but perform DFT calculations using a fairly large one-electron basis set with no ECPs so as to obtain reliable information about the structure (carbon distribution over the iron particle at low coverage), energetics, and magnetic states of $Fe_{13}C_n$, n = 1−20. The Fe_{13} cluster possesses a slightly distorted icosahedral structure[14−17] with practically equivalent faces. We started with a single carbon atom and added carbon atoms one by one until their total number reached 20, which is the number of triangular faces in the Fe_{13} icosahedral cluster. These faces are expected to be the preferred bonding sites according to the electron localization function (ELF) study[18] performed for Fe_4. Indeed, our computational studies have shown that the face attachment of O or N to Fe_4 and Fe_6 clusters[19,20] as well as C to a Fe_4 cluster[21] is preferred when the number of carbon atoms is small.

Our computations on $Fe_{13}C_n$ clusters (n = 1−20) are performed using an all-electron DFT method with generalized gradient approximation and a rather large basis set. We optimized also the ground-state C_n species (n = 2−20) at the same level of theory so that the energetics of the carbon−carbon binding in the gas phase could be compared to that in the presence of an Fe_{13} particle. To gain insight into the carbon chemisorption dependence on the spin multiplicity, we performed optimizations of Fe_{13} and $Fe_{13}C_8$ in the whole range of the spin multiplicities from 1 to 47.

Small precursors of these carbon allotropes were the subject of numerous experimental and theoretical investigations. Smalley

Received: January 12, 2012
Revised: February 23, 2012

   dx.doi.org/10.1021/jp300403p | J. Phys. Chem. C XXXX, XXX, XXX−XXX

et al.[22] studied the negatively charged C_n^- ions (n = 2−29) using ultraviolet photoelectron spectroscopy and concluded that the ground-state structures are linear chains up to n = 9, whereas the larger species possess monocyclic ring structures. They also found that the neutral even-numbered species possess open-shell electronic structures and high electron affinities, whereas the neutral odd-numbered species possess closed-shell singlet ground states and substantially lower electron affinities. Theoretical studies[23] confirmed the oscillatory character of the electron affinity in linear C_n^- up to n = 20. According to the experimental studies, linear and ring C_n^- ions do exist up to at least n = 16[24,25] and n = 41,[26] respectively. The smallest fullerene composed of 12 pentagons and 2 hexagons corresponds to n = 20, and the relative energetic stability of ring, bowl, and fullerene isomers of C_{20} has been the subject of many papers.[27−31] The total energy ordering of these isomers was found to be strongly dependent on the method and basis set used. According to a computational study[32] of relative energetic stabilities of C_n isomers for even n beginning with n = 18, a C_{24} fullerene is likely to be the smallest energetically favored fullerene.

The studies of interactions of carbon species with iron can be separated into several groups. The first group deals with interactions of a single Fe atom and a small number of carbon atoms, which includes FeC,[33−37] FeC_2,[38−40] FeC_3,[41,42] and FeC_n[43−49] with n = 4−10. The second group deals with interactions of small iron clusters with a small number of carbon atoms: Fe_2C_n (n = 3−4),[50] Fe_2C_3,[51] Fe_3C,[52] Fe_3C_2,[53] and Fe_nC (n = 4−6).[54,55] Some papers dealt with both FeC_n and Fe_mC_n.[56,57] Other groups include studies of endohedral complexes $Fe_n@C_{60}$,[58,59] Fe_nC_{12} (n = 2, 3, 4, 6.8, 10, 12),[60] metcars Fe_8C_{12},[61] and iron particle absorption on CNTs.[62]

The remainder of this paper is organized as follows. In Section II, we discuss the details of the computations. Section III presents and discusses our results. We summarize the main findings and conclude in Section IV.

II. DETAILS OF COMPUTATIONS

The Becke−Perdew−Wang exchange-correlation functional (BPW91)[63,64] and the 6-311+G* basis sets,[65] namely, (15s11p6d1f/10s7p4d1f) and (12s6p1d/5s4p1d) for iron and carbon atoms, respectively, were chosen to perform our calculations using the Gaussian 03 and 09 programs.[66,67] These choices are based on the results of our computational and joint computational and experimental studies of Fe_2CO,[68] MC (M = Sc to Zn),[69] Fe_n (n = 2−6),[70,71] Fe_nCO (n = 2−6),[72,73] CrC_n (n = 2−8),[74] and C_{60} fullerites,[75,76] which established that the BPW91/6-311+G* combination is capable to yield results in good agreement with experiment. For example, the spectroscopic constants obtained for the ground $^1\Sigma_g^+$ state of C_2 computed at this level of theory are r_e = 1.260 Å, ω_e = 1843 cm^{-1}, and D_o = 6.50 eV, which have to be compared to the experimental values[77] of r_e = 1.243 Å, ω_e = 1843 cm^{-1}, and D_o = 6.37 eV. A number of recently developed exchange-correlation functionals were intensively tested using different databases,[78,79] and the PW91 method is found to show a rather good performance compared to the new functionals.[80]

The ground-state geometrical configurations obtained for C_n (n = 2−20) in previous publications[81−93] were reoptimized at the BPW91/6-311+G* level to obtain total electronic energies and zero-point vibrational energies (ZPVE). The optimized ground states of C_n are as follows: C_2 ($^3\Pi_u$), C_3 ($^1\Sigma_g^+$), C_4 ($^3\Sigma_g^-$), C_5 ($^1\Sigma_g^+$), C_6 ($^3\Sigma_g^-$), C_7 ($^1\Sigma_g^+$), C_8 ($^3\Sigma_g^-$), C_9 ($^1\Sigma_g^+$), C_{10} ($^1A_1$), C_{11} ($^1A_1$), C_{12} (^1A_g), C_{13} ($^3B_1$), C_{14} (^1A_g), C_{15} ($^1A_1$), C_{16} (^1A_g), C_{17} ($^3B_1$), C_{18} (^1A_g), C_{19} ($^3B_1$), and C_{20} (^1A_g). The ground state of Fe_{13} was found to have a slightly distorted I_h geometry, and the spin multiplicity of 45 is in agreement with the results of previous computations. The use of the standard DFT method appears to be justified because of no noncollinear local magnetic moment was found[94,95] in iron clusters including Fe_{13}.

Our strategy in searching for the lowest total energy configurations of $Fe_{13}C_n$ is to add one carbon atom at a time and optimize as much carbon distributions as possible for each n. The initial distribution for a given number of carbon atoms was generated in three ways: (1) a random placement of single atoms over Fe_{13} face centers as uniformly as possible; (2) connected and disconnected single chains and rings; (3) adding a carbon atom to the previous optimal distribution as a single atom, forming a dimer, trimer, and so on. The optimizations of $Fe_{13}C_n$ were performed beginning with the spin multiplicity $2S + 1 = 41$ in the case of small carbon coverage since the quenching of the total magnetic moment was observed previously[96] for the Fe_4C_n clusters with n = 2−6. Optimizations were carried out for the states with the higher and lower spin multiplicities until the next spin multiplicity state showed a higher total energy. We found that the optimal spin multiplicity decreases to 37 when 6 carbon atoms are chemisorbed. No further decrease in the spin multiplicity of the lowest total energy state was observed for n > 6, except for few cases when the optimal spin multiplicity was 35.

Harmonic vibrational frequencies were computed for all C_n and $Fe_{13}C_n$ with $n \leq 10$, both to confirm that the structures were true energy minima (no imaginary frequencies) and to obtain the harmonic zero-point energies. Frequency calculations for larger n proved to be impractical with available computational resources. However, one has to expect that the total energy of a $Fe_{13}C_n$ isomer for a given n > 10 cannot be substantially lowered if the lowest total energy state found happened to correspond to a transition state. This conjecture is based on the observation that in most cases met for $n \leq 10$ the total energy lowering due to a transition state transformation into a stationary state by moving along the imaginary frequency mode has not exceeded 0.1−0.2 eV.

Fragmentation energies were computed as the differences in total energies of an initial species A and its decay products B_i

$$E_{diss} = E_{tot}^{el}(A) + ZPVE(A) - \sum_i [E_{tot}^{el}(B_i) + ZPVE(B_i)] \quad (1)$$

for A = C_n (n = 2−20) and $Fe_{13}C_n$ (n = 1−10), where ZPVE stands for the harmonic zero vibrational point energies. The difference of electronic total energies was used for $Fe_{13}C_n$ with n = 11−20

$$E_{diss} = E_{tot}^{el}(A) - \sum_i E_{tot}^{el}(B_i) \quad (2)$$

Local magnetic moments on atoms were obtained using both Mulliken[97] and Natural Atomic Orbital (NAO)[98] population analyses. Generally, the values obtained using both approaches are rather close to each other except for the central iron atom of Fe_{13}, where the Mulliken value appears to be unreliable. The NAO populations were used for analyzing the bonding patterns between Fe_{13} and carbon species.

dx.doi.org/10.1021/jp300403p | J. Phys. Chem. C XXXX, XXX, XXX−XXX

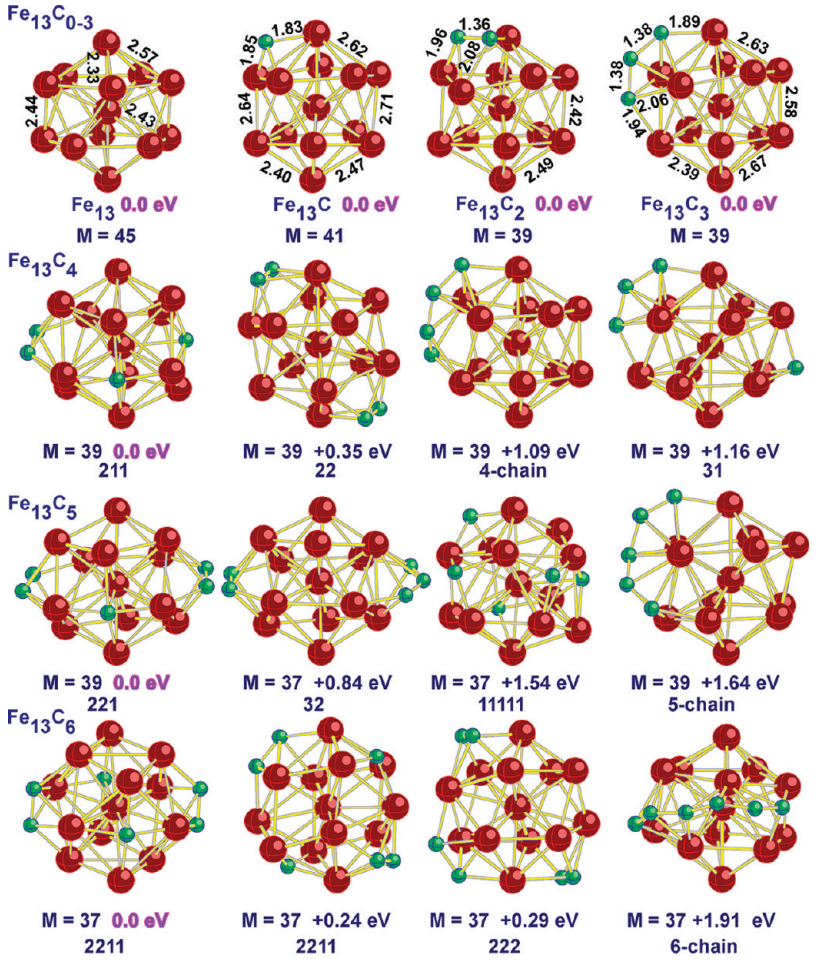

Figure 1. Geometrical configurations corresponding to the lowest total energy and selected excited states of $Fe_{13}C_n$ for n = 0−6. M denotes the multiplicity $2S + 1$. Bond lengths are in Å. The notation "n_in_j..." denotes the carbon chemisorption pattern, which corresponds to the separated carbon groups with n_i, n_j, ..., connected carbon atoms.

III. RESULTS AND DISCUSSION

First we present the lowest total energy structures found for $Fe_{13}C_n$ (n = 0−20) together with the isomers where carbon atoms are attached as a chain and two other selected isomers for each n, to emphasize the chemisorption pattern in the lowest total energy states. Next, we show that the dependence of total energy as a function of the spin multiplicity is similar for both Fe_{13} and $Fe_{13}C_8$ when moving down in the spin multiplicities to the singlet states. We discuss the bonding patterns and reasons for the quenching of the total magnetic moment of Fe_{13} by chemisorbed carbon and why the quenching does not depend on the coverage when the number of carbon atoms exceeds 6. Finally, we study thermodynamic patterns in the carbon chemisorption.

Geometrical Configurations. The geometrical configurations corresponding to the $Fe_{13}C_n$ states with different chemisorbed carbon topologies are presented in Figure 1 for n = 0−6. The pattern symbol denotes the presence of bonded carbon groups and/or single atoms on the iron cluster surface. For example, "211" means that there are one C_2 dimer and two single C atoms. The bond lengths shown for species with n = 0−3 are rather typical for the rest of the clusters: the Fe−Fe, Fe−C, and C−C bond lengths are in the range of 2.40−2.80 Å, 1.80−2.00 Å, and 1.35−1.45 Å, respectively.

The first carbon atom attaches to the center of one of 20 faces of Fe_{13} that are nearly equivalent since the I_h symmetry distortion is quite small. The second and third carbon atoms do attach in such a way as to form a carbon dimer and trimer, respectively. The $2S + 1 = 41$ state of $Fe_{13}C_2$ with two separated C atoms is above by 1.17 eV, whereas the $2S + 1 = 39$ states of $Fe_{13}C_3$ with a carbon dimer and a single atom and three separated C atoms are above by 0.37 and 0.74 eV, respectively. One could extrapolate that the next carbon atom attaches in such a way as to form a 4-atom chain, but it is not so. The lowest energy state of $Fe_{13}C_4$ corresponds to a "dimer + 2 singles" configuration of carbon atoms which is followed in total energy by the state whose carbon pattern is "22", whereas the state with a four-membered chain is above by 1.09 eV. A rather large separation in total energy of the "211" and "22" states can be related to a higher bonding ability of surface iron atoms of Fe_{13} which are not involved in bonding with previously chemisorbed carbon species. Thus, one can state that there is a competition between formation of a C−C bond with a chemisorbed carbon species and the bonding to free iron atoms.

Let us consider in detail why the C_2 dimer formation is energetically preferable over the chemisorption of two separated carbon atoms. The formation energy of a C_2 dimer, when the dimer is formed by adding a carbon atom to $Fe_{13}C$, is estimated as the decay energy of the lowest total energy state of $Fe_{13}C_2$ (see Figure 1) to $Fe_{13}C$ + C. The value of 7.14 eV obtained in this way can be compared to the value of 6.50 eV

dx.doi.org/10.1021/jp300403p | J. Phys. Chem. C XXXX, XXX, XXX−XXX

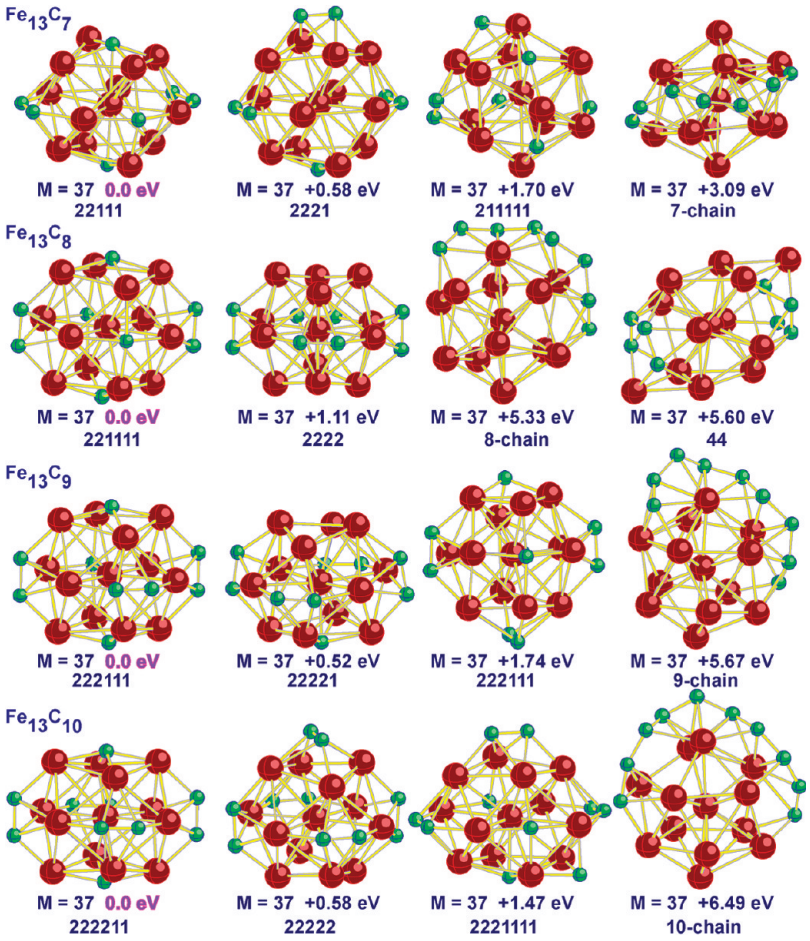

Figure 2. Geometrical configurations corresponding to the lowest total energy and selected excited states of $Fe_{13}C_n$ for n = 7−10. "n-chain" denotes a chain consisting of n connected carbon atoms.

for the gas phase $C_2 \rightarrow 2C$ dissociation. Note that our computed energy for a single C atom attachment to a bare Fe_{13} cluster is 6.68 eV. The dissociation energy for the $Fe_{13}C_2 \rightarrow C_2$ channel is 7.32 eV, thus making the formation energy of a C_2 dimer on the iron cluster 14.46 eV compared to ∼2*6.68 eV = 13.36 eV for the separate attachment of two carbon atoms. The latter value is smaller by 0.07 eV than the difference of 1.17 eV in total energies of the $Fe_{13}C_2$ ground and $Fe_{13}C_2$ (11) isomer states; that is, there is almost no interaction between two carbon atoms placed on the cluster surface opposite to each other. Assuming that the chemisorption energy of a single carbon atom in the lowest total energy state of $Fe_{13}C_4$ (211) is the same as in $Fe_{13}C$, i.e., 6.68 eV, one can estimate the fragmentation energy for $Fe_{13}C_4$ (211) → $Fe_{13}C_2$ (2) + 2C as ∼13.36 eV, while the fragmentation energy for $Fe_{13}C_4$ (4) → $Fe_{13}C_2$ (2) + 2C is 12.43 eV. The smaller energy value in the second case can be related to a weaker bonding of the C_4 chain since the C−C and Fe−C bonding energies are quite similar.

When increasing the number of carbon atoms to 12, one observes formation of an octahedron composed of C_2, with Fe_{13} being endohedral (compare Figures 1−3). A similar carbon distribution was found[60] in the spin-restricted computations for the first excited state of $Fe_{12}C_{12}$ where Fe_{12} possesses an I_h shell structure. The lowest energy state of $Fe_{12}C_{12}$ was found to possess a "tower" shape[99] of an iron carbide type composed from four-membered Fe_2C_2 rings. In our optimizations of the tower-type isomer of $Fe_{13}C_{13}$, we observed the formation of a C_2 dimer on the tower top; however, the isomer states with the spin multiplicities ranging from 31 to 41 were found to be above the lowest energy state by 7−8 eV.

As is seen from Figures 1−3, the difference between total energies of the lowest total energy states and the states of isomers of $Fe_{13}C_n$ containing carbon chains grows as n increases. The "322221" isomer state of $Fe_{13}C_{12}$ (see Figure 3) is close in total energy to the lowest energy "222222" state. This implies that the next structural pattern would be the formation of carbon trimers up to an octahedron composed of the trimers at n = 18. Indeed, our search confirmed that the most energetically preferable geometry trend is the gradual formation of carbon trimers by adding carbon atoms to the dimers of the ground-state $Fe_{13}C_{12}$ cluster.

For $Fe_{13}C_{16}$, we have also optimized a structure composed of two C_8 placed on Fe_{13} one over another. The result of our optimizations is presented in Figure 4. As is seen, the top eight carbon atoms retain the 8-membered ring shape, whereas adding one more atom transforms this carbon structure to a cap containing hexagons and pentagons (see Figure 4, the bottom panel). However, adding two atoms conserves the top eight-membered ring in the "CNT" isomer of $Fe_{13}C_{18}$ (see Figure 5). Note that the state whose geometry is presented by the carbon ring encircling the Fe_{13} cluster is higher in total energy by 4.97 eV than the lowest energy state, whereas the chain broken into two pieces "8−10" is higher by 4.67 eV. This means that the energy gain due to formation of a C−C bond

dx.doi.org/10.1021/jp300403p | J. Phys. Chem. C XXXX, XXX, XXX−XXX

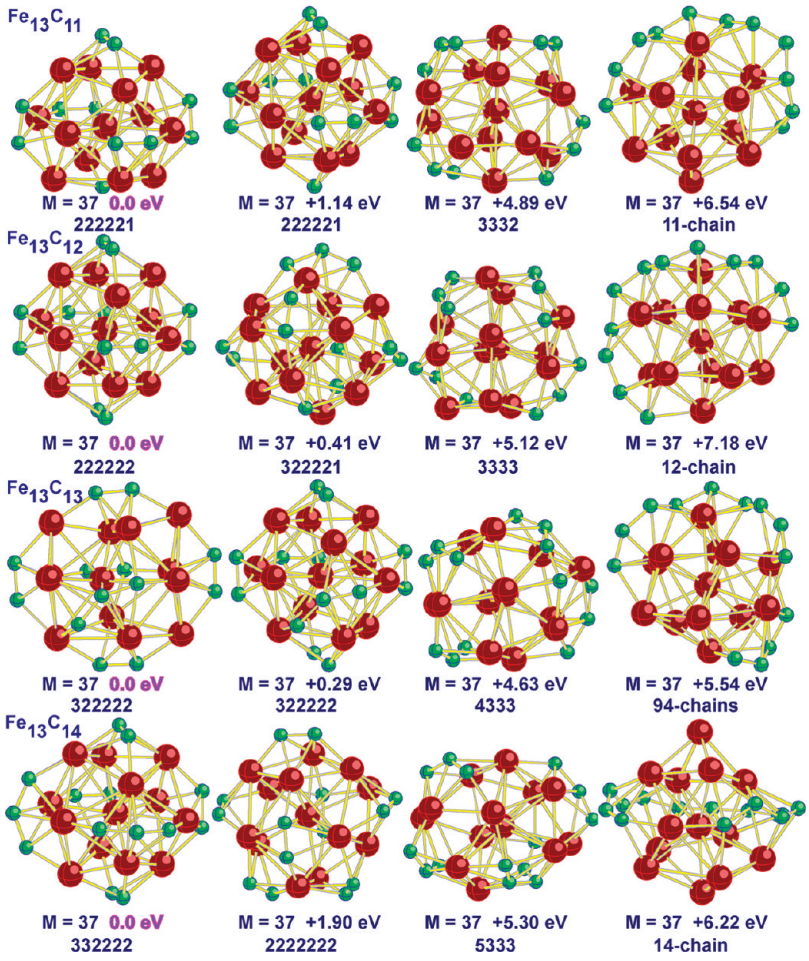

Figure 3. Geometrical configurations corresponding to the lowest total energy and selected excited states of $Fe_{13}C_n$ for n = 11−14.

in the ring exceeds the sum of the binding energies of four end atoms of the eight-membered and ten-membered carbon chains by 0.3 eV.

The state of a $Fe_{13}C_{18}$ isomer with a "433332" carbon pattern is higher in total energy than the "333333" state by only 0.04 eV (see Figure 6), which assumes that carbon tetramers could continue the series of "six dimers" and "six trimers". However, only $Fe_{13}C_{19}$ follows this assumption. The lowest energy state found for $Fe_{13}C_{20}$ using initial random distributions of carbon atoms has a "53332211" type; i.e., it contains a carbon pentamer, three carbon tetramers, three carbon dimers, and two single carbon atoms. The state whose geometry contains two carbon tetramers is higher in total energy by 0.42 eV; the state whose geometry is presented by a 20-membered carbon ring wrapped around the iron cluster is higher by 1.65 eV; and the state whose geometry contains a C_{20} bowl is higher by 2.62 eV. Note that the iron particle geometry in the lowest energy state of $Fe_{13}C_{20}$ is strongly distorted, whereas it is not so for higher energy isomers.

Spin Dependence. The total magnetic moment of a given state is defined in the Russell−Saunders scheme as $\boldsymbol{\mu} = \mu_B(\mathbf{L} + 2\mathbf{S})$, where μ_B is the Bohr magneton and **L** and **S** are the total angular and spin moments, respectively. Within the Heisenberg model, one neglects the **L** contribution and defines $\mu = g_e\mu_B S$, where the gyromagnetic ratio g_e is 2.0023 and μ_B is the Bohr magneton. The total spin is $S = (n_\alpha - n_\beta)/2$, where n_α and n_β are the numbers of the spin-up and spin-down electrons, respectively. We accept the local magnetic moments on atoms to be equal to the excess spin density obtained using the NAO populations.

To gain insight into how carbon chemisorption is related to the spin multiplicity, we performed optimizations of the Fe_{13} and $Fe_{13}C_8$ clusters in the range of spin multiplicities $2S + 1$ from 1 to 47. The relative total energies ΔE_{tot} computed with respect to the total energies of the corresponding lowest energy states are presented in Figure 7. For clarity, the curves for $0 \leq (2S + 1) \leq 23$ are presented in the lower panel and $24 \leq (2S + 1) \leq 47$ in the upper panel. As is seen, the minimum energy for the Fe_{13} cluster occurs for $2S + 1 = 45$, while the minimum for $Fe_{13}C_8$ is at $2S + 1 = 37$. As one moves down in spin multiplicities, there is a rather fast rise in ΔE_{tot} when moving to $2S + 1 = 33$ for both cases. Both series show small oscillations around the value of 1.5 eV for smaller spin multiplicities. The largest ΔE_{tot} values correspond to $2S + 1 = 25$ and 19 for both Fe_{13} and $Fe_{13}C_8$, which are the spin multiplicities at which the local magnetic moment of one iron atom flips. In terms of the excess spin density at this atom, it means that the populations of the spin-down and spin-up atomic orbitals are reversed. The average electronic configuration of an Fe atom in Fe_{13}, except for the central atom where the population is $\sim 3d^{8.0}4s^{1.0}$, is $\sim 3d^{6.8}4s^{0.8}$ and corresponds to a practically inert $3d^{4.9}$ subshell and a valence $4s^{0.4}$ component in one spin representation and the valence $3d^{1.8}4s^{0.4}$ population in the second spin representation. The corresponding excess spin density is 3.1 e.

The flipping of local magnetic moments leads to the change in the valence interactions and to a higher total energy of the

dx.doi.org/10.1021/jp300403p | J. Phys. Chem. C XXXX, XXX, XXX−XXX

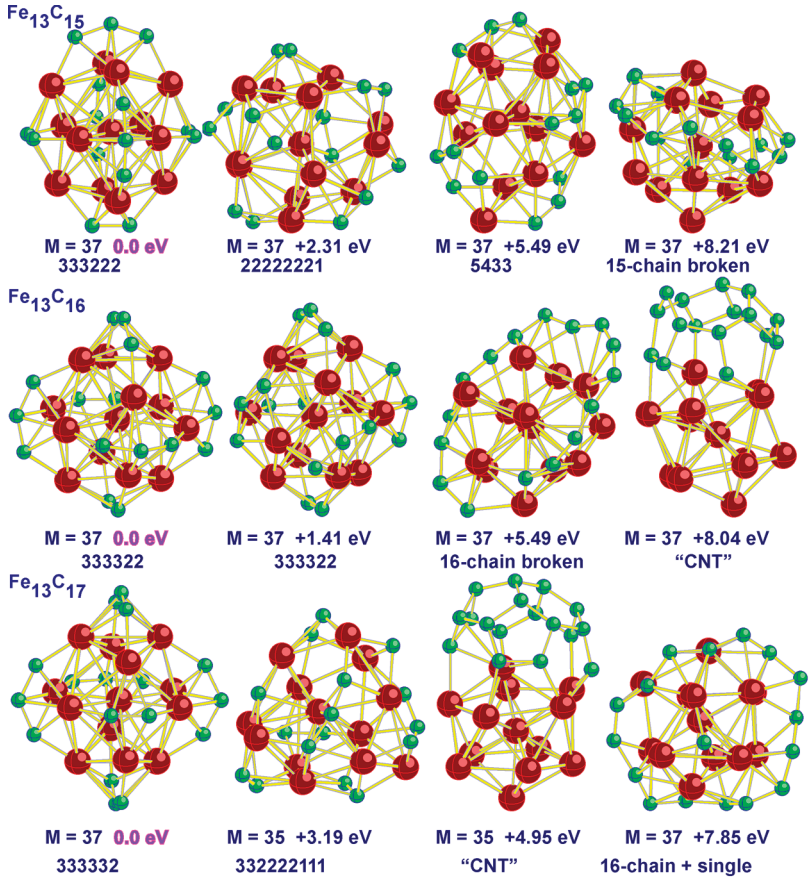

Figure 4. Geometrical configurations corresponding to the lowest total energy and selected excited states of $Fe_{13}C_n$ for n = 12−17. "CNT" denotes a structure resembling the cap of a SWCNT.

corresponding cluster state. Other flipping points also show a small increase in total energy with respect to their neighbors but to a lesser extent than in the $2S + 1 = 25$ and 19 cases. As one moves to higher spin multiplicities from the respective minima of Fe_{13} and $Fe_{13}C_8$, ΔE_{tot} grows rapidly in the both series. Since the ΔE_{tot} behavior is nearly the same as in the Fe_{13} and $Fe_{13}C_8$ series, one can conclude that the binding capability of Fe_{13} does not nearly depend on the spin multiplicity when $2S + 1 < 35$.

To gain insight into the nature of the total magnetic moment quenching due to carbon chemisorption, we analyze changes in the Fe NAO populations due to the chemisorption. In the ground state of Fe_{13}, the effective electronic configuration of an outer Fe atom is $(3d^{6.84}4s^{0.98}) = [3d^{4.96}4s^{0.69}]\alpha\ [3d^{1.89}4s^{0.30}]\beta$, and the central atom has an effective electronic configuration of $[3d^{4.93}4s^{0.44}]\alpha\ [3d^{2.68}4s^{0.47}]\beta$. That is, the α 3d-subshell is chemically inert, and the bonding is due to the 4s and 3dβ electrons which corresponds to the valence of an Fe atom of ~3. Table 1 presents the NAO populations for an isomer and the lowest total energy state of $Fe_{13}C_8$ with $2S + 1 = 37$. As is seen, the NAO populations of both isomers are quite similar. The effective electronic configuration of a carbon atom is $\sim[2s^{1.20}2p^{3.1}]$ with nearly the same occupation in the α- and β-spin representations. That is, the effective electronic configurations of carbon atoms correspond to an sp^3-hybridization of the valence AOs with the total charge transfer of ~2.5 e from iron atoms. Since the 4s-population of iron atoms in the bare Fe_{13} cluster is ~1 e, the effective electronic configurations of iron atoms in $Fe_{13}C_8$ correspond to a transfer of ~0.3 e to carbon atoms and the promotion of ~0.4 e into the Fe 4p-states. Note that the distributions of the Fe 4s and 4p NAOs in the α- and β-spin representations are nearly symmetric, which means that the total magnetic moment of the cluster is defined by the sum of the differences between 3dα and 3dβ populations. The average difference is ~2.7 e, which results in the total magnetic moment of $\sim 2.7 \times 13 = 35\ \mu_B$, and the corresponding state has the spin multiplicity of 35 or 37. Note also that α-3d populations of iron atoms are somewhat smaller than the 3dα populations in the bare Fe_{13} cluster, which means that this shell participates in the bonding. Depletion of the Fe 4s electrons and the decrease in the Fe 3dα population by approximately the same amount as in the $Fe_{13}C_8$ isomers considered are typical for other $Fe_{13}C_n$ clusters that explains why their lowest total energy states possess the same spin multiplicity of 37 or, occasionally, 35.

Spin contamination was found[100] to be rather small in ferromagnetic states of FeO_n, whereas it was found to be large in antiferromagnetic low-spin states. The same trend is observed for the Fe_{13} and $Fe_{13}C_8$ clusters. The computed $\langle S^2 \rangle$ value of the Fe_{13} ground state is 506.334; the projected value is 506.004; and the exact $S(S + 1)$ value is 506. That is, the spin contamination is only 0.07%. The spin contamination does not increase substantially due to carbon chemisorption. The computed $\langle S^2 \rangle$ value of the $Fe_{13}C_8$ lowest total energy state with $2S + 1 = 37$ is 342.478; the projected value is 342.012; and the exact value is 342; i.e., the corresponding spin contamination is 0.14%. In antiferromagnetic states of Fe_{13} and $Fe_{13}C_8$, the spin contamination is substantially higher.

dx.doi.org/10.1021/jp300403p | J. Phys. Chem. C XXXX, XXX, XXX−XXX

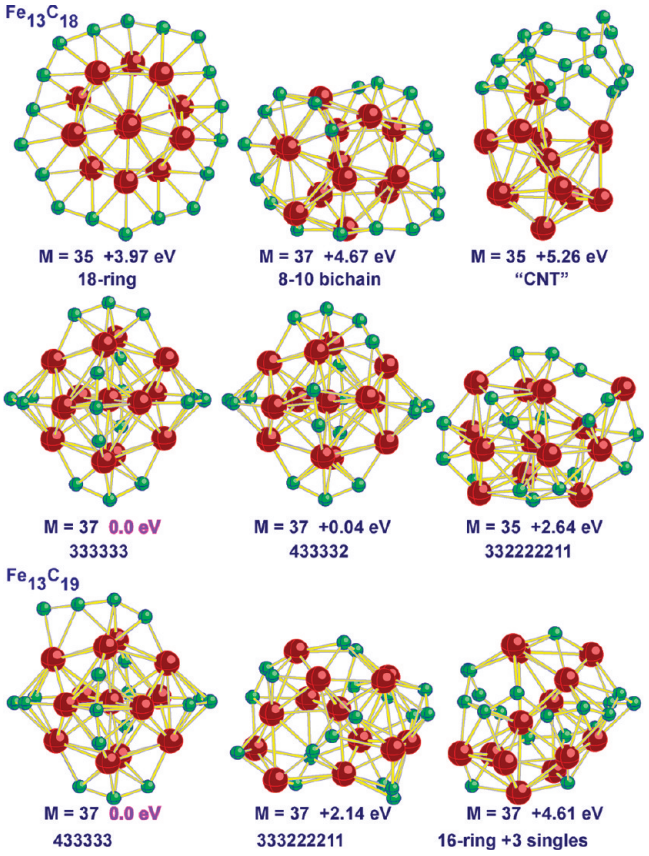

Figure 5. Geometrical configurations corresponding to the lowest total energy and selected excited states of $Fe_{13}C_{18}$ and $Fe_{13}C_{19}$.

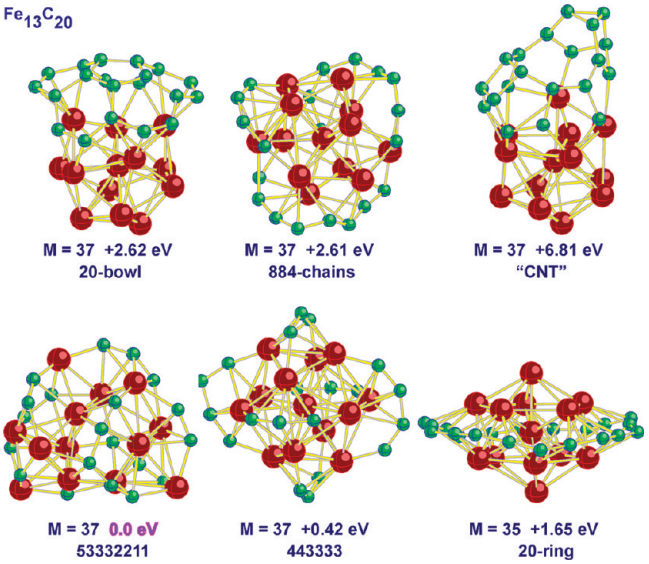

Figure 6. Isomers of $Fe_{13}C_{20}$.

Vibrational Frequencies. As an example, we compare harmonic vibrational frequencies of ground-state C_8 ($^3\Sigma_g^-$), Fe_{13} ($2S + 1 = 45$), and $Fe_{13}C_8$ (2222 and 221111) in Table 2. As is seen, the vibrational frequencies of the $Fe_{13}C_8$ isomers are similar to those of the bare Fe_{13} clusters at the smaller vibrational frequency side, and there is no vibrational frequency corresponding to a single C_2 dimer (~1800 cm^{-1} in the gas phase, 1384 cm^{-1} in $Fe_{13}C_2(2)$ in Fib. 1). The largest four

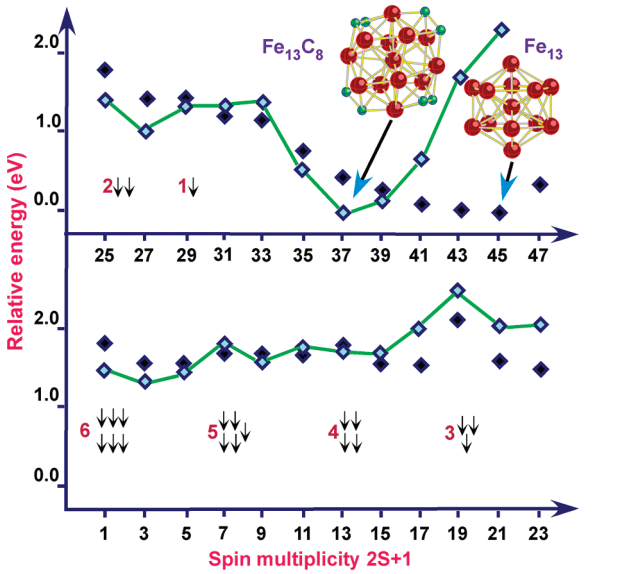

Figure 7. Relative energies of Fe_{13} and $Fe_{13}C_8$ (2222) as functions of the spin multiplicity. The number in the front of the arrow sets corresponds to the number of the spin-down local magnetic moments on iron atoms at the given spin multiplicity.

vibrational frequencies in the $Fe_{13}C_8$ (2222) isomer do correspond to two nearly degenerate modes of the e-type vibrations of the opposite pairs of C_2 dimers. The same type of vibration is found for two pairs of C_2 dimers in the lowest total energy state of $Fe_{13}C_8$ with the "221111" geometrical pattern. One mode at 1513 cm^{-1} corresponds to the in-phase stretching of bonds of the dimers, and the second mode corresponds to the antiphase stretching mode.

Thermodynamic Properties. To estimate the thermodynamic stability of $Fe_{13}C_n$, we have computed the energies of decay through various channels according to eqs 1 and 2. We consider first the energetics of a single carbon atom abstraction from the ground states of C_n and $Fe_{13}C_n$ and the full carbon stripping off a $Fe_{13}C_n$ cluster [the channel $Fe_{13}C_n \rightarrow Fe_{13} + C_n$ (g. s.)]. As follows from Figure 8, the $C_n \rightarrow C_{n-1} + C$ abstraction energy curve as a function of n possesses a sawtooth shape with the prominent peaks at $n = 10$, 14, and 18. These n values correspond to the most stable cumulene structures defined by the relationship $n = 4k + 2$.[101] The $Fe_{13}C_n \rightarrow Fe_{13}C_{n-1} + C$ energies show slow variations around 7 eV and decrease to 6 eV at $n = 18-20$. The $C_n \rightarrow C_{n-1} + C$ energies possess much larger fluctuations: from 8.4 eV at $n = 18$ to 5.4 eV at $n = 19$ and 6.5 eV at $n = 20$. The $Fe_{13}C_n \rightarrow Fe_{13} + C_n$ decay energies exceed 9 eV for $n = 7-17$ and drop to ~7 eV at $n = 20$. The absolute maximum of 11.9 eV corresponds to $n = 12$ which is in line with the experimental observation[102] of the prominent features of $Fe_nO_m^+$ species when the stoichiometric ratio is 1:1.

Figure 9 presents the energies of partial removal of carbon from $Fe_{13}C_n$ according to the decay channels $Fe_{13}C_n \rightarrow Fe_{13}C_{n-k} + C_k$, $k = 2-7$, where the corresponding species are in the lowest energy states. As is seen, curve (b) corresponding to the abstraction of a C_3 trimer is below all other curves for n up to $n = 18$. This curve is closely followed by curve (a), which corresponds to abstraction of a C_2 dimer, by $n = 15$. All curves show a similar behavior: they possess maximal values at $n = 8-12$ and approach the values between 3.2 and 4.4 eV at $n = 20$, except for the $Fe_{13}C_n \rightarrow Fe_{13}C_{n-2} + C_2$ channel, where the $n = 20$ value is 5.81 eV.

dx.doi.org/10.1021/jp300403p | J. Phys. Chem. C XXXX, XXX, XXX−XXX

Table 1. Natural Atomic Orbital Populations on Atoms in Two Isomers of $Fe_{13}C_8$ with $2S + 1 = 37$[a]

		iomer (2222) of $Fe_{13}C_8$			lwest energy state (221111) of $Fe_{13}C_8$		
		total	spin-up	spin-down	total	spin-up	spin-down
1	C	$2s^{1.2}2p^{3.1}$	$2s^{0.6}2p^{1.6}$	$2s^{0.6}2p^{1.6}$	$2s^{1.2}2p^{3.1}$	$2s^{0.6}2p^{1.6}$	$2s^{0.6}2p^{1.5}$
2	C	$2s^{1.2}2p^{3.1}$	$2s^{0.6}2p^{1.6}$	$2s^{0.6}2p^{1.6}$	$2s^{1.2}2p^{3.1}$	$2s^{0.6}2p^{1.6}$	$2s^{0.6}2p^{1.5}$
3	C	$2s^{1.2}2p^{3.1}$	$2s^{0.6}2p^{1.6}$	$2s^{0.6}2p^{1.6}$	$2s^{1.2}2p^{3.1}$	$2s^{0.6}2p^{1.6}$	$2s^{0.6}2p^{1.5}$
4	C	$2s^{1.2}2p^{3.1}$	$2s^{0.6}2p^{1.6}$	$2s^{0.6}2p^{1.6}$	$2s^{1.2}2p^{3.1}$	$2s^{0.6}2p^{1.6}$	$2s^{0.6}2p^{1.5}$
5	C	$2s^{1.2}2p^{3.1}$	$2s^{0.6}2p^{1.6}$	$2s^{0.6}2p^{1.6}$	$2s^{1.2}2p^{3.2}$	$2s^{0.6}2p^{1.7}$	$2s^{0.6}2p^{1.6}$
6	C	$2s^{1.2}2p^{3.1}$	$2s^{0.6}2p^{1.6}$	$2s^{0.6}2p^{1.6}$	$2s^{1.2}2p^{3.2}$	$2s^{0.6}2p^{1.7}$	$2s^{0.6}2p^{1.6}$
7	C	$2s^{1.2}2p^{3.1}$	$2s^{0.6}2p^{1.6}$	$2s^{0.6}2p^{1.6}$	$2s^{1.3}2p^{3.2}$	$2s^{0.7}2p^{1.6}$	$2s^{0.6}2p^{1.6}$
8	C	$2s^{1.2}2p^{3.1}$	$2s^{0.6}2p^{1.6}$	$2s^{0.6}2p^{1.6}$	$2s^{1.3}2p^{3.2}$	$2s^{0.7}2p^{1.6}$	$2s^{0.6}2p^{1.6}$
9	Fe	$4s^{0.4}3d^{7.4}4p^{1.4}$	$4s^{0.2}3d^{4.9}4p^{0.7}$	$4s^{0.2}3d^{2.5}4p^{0.7}$	$4s^{0.3}3d^{7.5}4p^{1.1}$	$4s^{0.2}3d^{4.8}4p^{0.6}$	$4s^{0.1}3d^{2.5}4p^{0.5}$
10	Fe	$4s^{0.3}3d^{6.9}4p^{0.4}$	$4s^{0.2}3d^{4.8}4p^{0.2}$	$4s^{0.1}3d^{2.1}4p^{0.2}$	$4s^{0.3}3d^{6.9}4p^{0.5}$	$4s^{0.2}3d^{4.8}4p^{0.3}$	$4s^{0.1}3d^{2.1}4p^{0.2}$
11	Fe	$4s^{0.3}3d^{7.0}4p^{0.5}$	$4s^{0.2}3d^{4.7}4p^{0.3}$	$4s^{0.1}3d^{2.3}4p^{0.2}$	$4s^{0.3}3d^{6.9}4p^{0.5}$	$4s^{0.2}3d^{4.8}4p^{0.2}$	$4s^{0.1}3d^{2.2}4p^{0.2}$
12	Fe	$4s^{0.3}3d^{6.9}4p^{0.4}$	$4s^{0.2}3d^{4.9}4p^{0.2}$	$4s^{0.1}3d^{2.1}4p^{0.2}$	$4s^{0.3}3d^{7.0}4p^{0.4}$	$4s^{0.2}3d^{4.7}4p^{0.3}$	$4s^{0.1}3d^{2.4}4p^{0.2}$
13	Fe	$4s^{0.3}3d^{6.9}4p^{0.4}$	$4s^{0.2}3d^{4.9}4p^{0.2}$	$4s^{0.1}3d^{2.1}4p^{0.2}$	$4s^{0.3}3d^{7.0}4p^{0.4}$	$4s^{0.2}3d^{4.7}4p^{0.3}$	$4s^{0.1}3d^{2.4}4p^{0.2}$
14	Fe	$4s^{0.3}3d^{6.9}4p^{0.4}$	$4s^{0.2}3d^{4.8}4p^{0.2}$	$4s^{0.1}3d^{2.1}4p^{0.2}$	$4s^{0.3}3d^{6.9}4p^{0.5}$	$4s^{0.2}3d^{4.8}4p^{0.3}$	$4s^{0.1}3d^{2.1}4p^{0.2}$
15	Fe	$4s^{0.3}3d^{7.0}4p^{0.5}$	$4s^{0.2}3d^{4.7}4p^{0.3}$	$4s^{0.1}3d^{2.3}4p^{0.2}$	$4s^{0.3}3d^{6.9}4p^{0.4}$	$4s^{0.2}3d^{4.8}4p^{0.2}$	$4s^{0.1}3d^{2.2}4p^{0.2}$
16	Fe	$4s^{0.3}3d^{6.9}4p^{0.4}$	$4s^{0.2}3d^{4.9}4p^{0.2}$	$4s^{0.1}3d^{2.1}4p^{0.2}$	$4s^{0.3}3d^{7.0}4p^{0.4}$	$4s^{0.2}3d^{4.7}4p^{0.2}$	$4s^{0.1}3d^{2.4}4p^{0.2}$
17	Fe	$4s^{0.3}3d^{6.9}4p^{0.4}$	$4s^{0.2}3d^{4.9}4p^{0.2}$	$4s^{0.1}3d^{2.1}4p^{0.2}$	$4s^{0.3}3d^{7.0}4p^{0.4}$	$4s^{0.2}3d^{4.7}4p^{0.2}$	$4s^{0.1}3d^{2.4}4p^{0.2}$
18	Fe	$4s^{0.3}3d^{7.0}4p^{0.5}$	$4s^{0.2}3d^{4.7}4p^{0.3}$	$4s^{0.1}3d^{2.3}4p^{0.2}$	$4s^{0.3}3d^{6.9}4p^{0.4}$	$4s^{0.2}3d^{4.8}4p^{0.2}$	$4s^{0.1}3d^{2.2}4p^{0.2}$
19	Fe	$4s^{0.3}3d^{6.9}4p^{0.4}$	$4s^{0.2}3d^{4.8}4p^{0.2}$	$4s^{0.1}3d^{2.1}4p^{0.2}$	$4s^{0.3}3d^{6.9}4p^{0.5}$	$4s^{0.2}3d^{4.8}4p^{0.3}$	$4s^{0.1}3d^{2.1}4p^{0.2}$
20	Fe	$4s^{0.3}3d^{6.9}4p^{0.4}$	$4s^{0.2}3d^{4.8}4p^{0.2}$	$4s^{0.1}3d^{2.1}4p^{0.2}$	$4s^{0.3}3d^{6.9}4p^{0.5}$	$4s^{0.2}3d^{4.8}4p^{0.3}$	$4s^{0.1}3d^{2.1}4p^{0.2}$
21	Fe	$4s^{0.3}3d^{7.0}4p^{0.5}$	$4s^{0.2}3d^{4.7}4p^{0.3}$	$4s^{0.1}3d^{2.3}4p^{0.2}$	$4s^{0.3}3d^{6.9}4p^{0.4}$	$4s^{0.2}3d^{4.8}4p^{0.2}$	$4s^{0.1}3d^{2.2}4p^{0.2}$

[a]The NAO populations are rounded to the first decimal after the point; populations of excited AOs that are smaller than 0.05 are not shown. Atom No. 9 is the central atom of the Fe_{13} cluster.

Table 2. Comparison of Harmonic Vibrational Frequencies (in cm^{-1}) of C_8 (g. s.), Fe_{13} (g. s.), and Two Isomers of $Fe_{13}C_8$

	vibrational frequencies (in cm^{-1})
C_8 ($^1\Delta$, π_g^2)	61, 61, 134, 134, 210, 210, 349, 349, 471, 471, 500, 610, 610, 944, 1355, 1713, 1971, 2095, 2111
Fe_{13}, $2S + 1 = 45$	32, 89, 90, 97, 98, 101, 102, 106, 106, 129, 130, 131, 147, 151, 152, 154, 154, 191, 191, 196, 197, 207, 208, 218, 233, 233, 255, 259, 260, 275, 358, 359, 360
$Fe_{13}C_8$, $2S + 1 = 37$ (2222)	78, 83, 107, 109, 118, 120, 121,129,136, 142, 142, 149, 156, 156, 160, 163, 170, 171, 181, 195, 200, 204, 207, 211, 224, 228, 243, 246, 248, 255, 291, 300, 300, 343, 348, 372, 380, 392, 400, 400, 409, 416, 419, 421, 430, 457, 459, 461, 461, 490, 495, 500, 517, 1396, 1400, 1436, 1442
$Fe_{13}C_8$, $2S + 1 = 37$ (221111)	90, 113, 118, 123, 126, 130, 123, 126, 130, 135, 143, 152, 156, 158, 160, 166, 166, 167, 174, 176, 194, 197, 203, 205, 213, 215, 217, 228, 233, 240, 250, 259, 271, 272, 283, 292, 346, 355, 372, 382, 390, 408, 436, 446, 458, 469, 472, 505, 515, 519, 520, 540, 578, 596, 633, 635, 654, 674, 1513, 1535

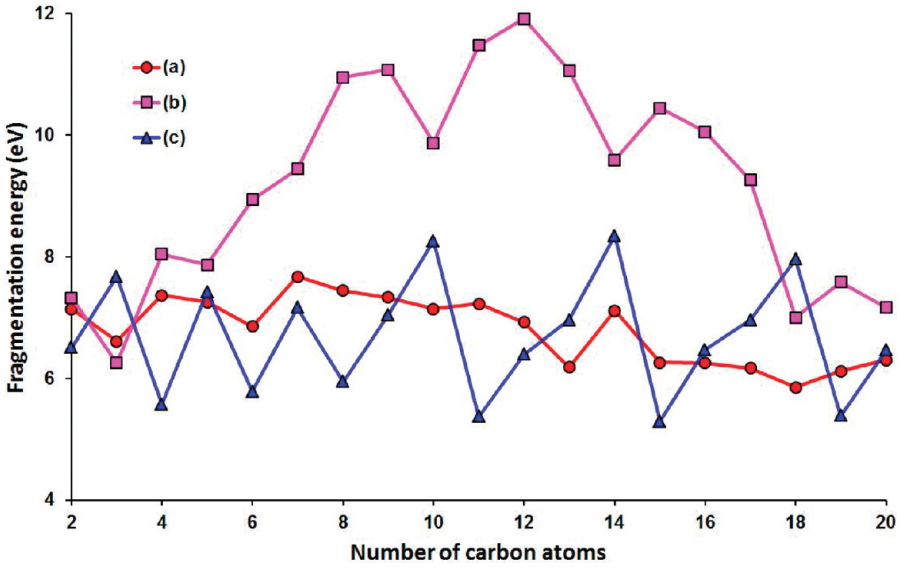

Figure 8. Fragmentation energies through the channels: (a) $Fe_{13}C_n \rightarrow Fe_{13}C_n + C$; (b) $Fe_{13}C_n \rightarrow Fe_{13} + C_n$; (c) $C_n \rightarrow C_{n-1} + C$.

Comparison of fragmentation energies for the $Fe_{13}C_n \rightarrow Fe_{13}C_{n-k} + C_k$ and $C_n \rightarrow C_{n-k} + C_k$ channels for $k = 8-10$ is presented in Figure 10. As is seen, the behavior of the $Fe_{13}C_n$ decay curves is similar to that in Figure 9. The curve maxima

dx.doi.org/10.1021/jp300403p | J. Phys. Chem. C XXXX, XXX, XXX−XXX

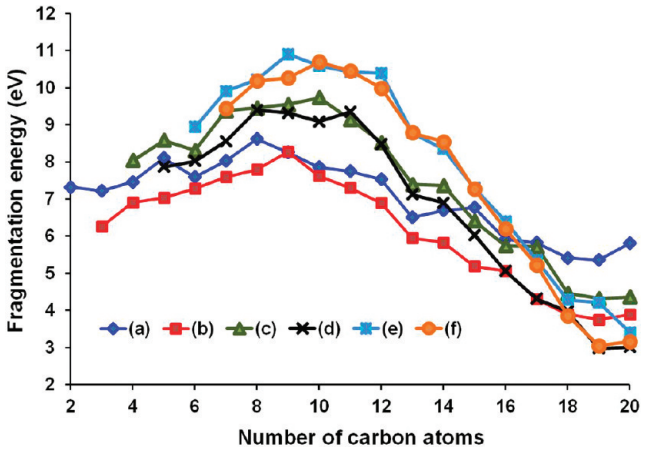

Figure 9. Fragmentation energies of $Fe_{13}C_n \rightarrow Fe_{13}C_{n-k} + C_k$: (a) $k = 2$; (b) $k = 3$; (c) $k = 4$; (d) $k = 5$; (e) $k = 6$; (f) $k = 7$.

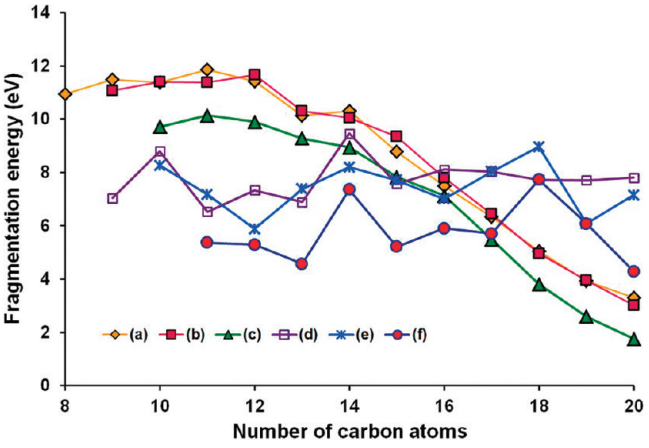

Figure 10. Fragmentation energies of $Fe_{13}C_n \rightarrow Fe_{13}C_{n-k} + C_k$: (a) $k = 8$; (b) $k = 9$; (c) $k = 10$; and fragmentation energies of $C_n \rightarrow C_{n-k} + C_k$: (d) $k = 8$; (e) $k = 9$; (f) $k = 10$.

are shifted to larger n, and the smallest energy of 1.76 eV is observed for the $Fe_{13}C_{20} \rightarrow Fe_{13}C_{10} + C_{10}$ channel. The $C_n \rightarrow C_{n-k} + C_k$ curves possess spikes at the cumulene values of n, and they have no monotonic decrease at larger n. The smallest value of 4.29 eV in the C_n decay series belongs to the $C_{20} \rightarrow C_{10} + C_{10}$ channel, which is to be related with the high stability of C_{10} possessing a cumulene structure. The same is true for the $Fe_{13}C_{20} \rightarrow Fe_{13}C_{10} + C_{10}$ channel. The energy decrease in the $Fe_{13}C_n \rightarrow Fe_{13}C_{n-k} + C_k$ channels is related to the decreasing stability of $Fe_{13}C_n$ at larger n. The behavior of dissociation energies for $n > 10$ is rather similar for all $Fe_{13}C_n \rightarrow Fe_{13}C_{n-k} + C_k$ channels. As is seen from Figure 11, the energies decrease nearly monotonically as n increases. At $n = 20$, the smallest dissociation energy of 3.42 eV belongs to the $Fe_{13}C_{20} \rightarrow Fe_{13}C_9 + C_{11}$ channel, and the largest dissociation energy of 7.16 eV belongs to the channel $Fe_{13}C_{20} \rightarrow Fe_{13} + C_{20}$.

Now we compare atomization energies of the carbon species chemisorbed on Fe_{13} in the lowest total energy states of $Fe_{13}C_n$ with atomization energies of the ground-state C_n species to gain insight into the carbon binding capability of Fe_{13} for $n = 1-20$. These atomization energies are displayed in Table 3 where the second column presents the content of carbon chemisorbed on Fe_{13}, and the third column shows the corresponding fragmentation channels. Column **4** presents the fragmentation

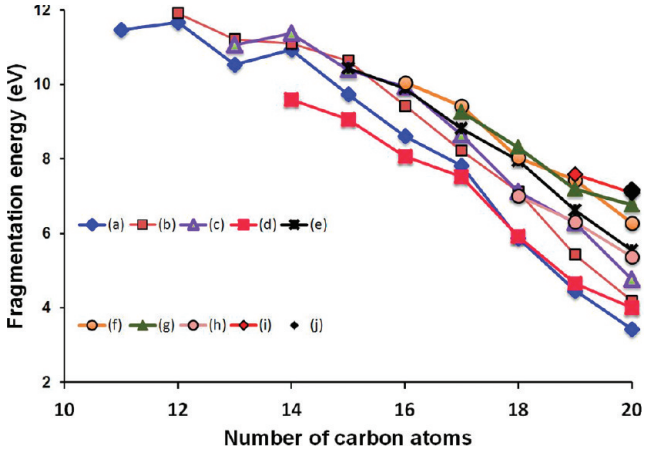

Figure 11. Fragmentation energies of $Fe_{13}C_n \rightarrow Fe_{13}C_{n-k} + C_k$: (a) $k = 11$; (b) $k = 12$; (c) $k = 13$; (d) $k = 14$; (e) $k = 15$; (f) $k = 16$; (g) $k = 17$; (h) $k = 18$; (i) $k = 19$; (j) $k = 19$.

energies D_0 or D_e, i.e., with taking into account the $Fe_{13}C_n$ ZPVEs for $n \leq 10$ (D_0) and without the ZPVEs for larger n (D_e). The ZPVE contribution is expected to be around 0.15 eV. The next column presents atomization energies of carbon species in the right-hand side of the fragmentation channels in column **3**, and column **6** contains the sum of fragmentation and atomization energies from columns **4** and **5**. Column **7** presents the atomization energies of the gas-phase C_n species.

As is seen, the binding energy of carbon species and Fe_{13} reaches a local maximum at $n = 12$ and decreases at larger n except for the 5333221 isomer of $Fe_{13}C_{20}$. The sum $\Delta E_{tot}(Fe_{13}C_n \rightarrow Fe_{13} + \sum C_i) + \Delta E_{tot}(\sum C_i \rightarrow nC)$ values presented in column **6** have to be compared to the $\Delta E_{tot}(C_n \rightarrow nC)$ atomization energies given in column **7**. Comparison shows that atomization energies of carbon chemisorbed on Fe_{13} are larger by approximately 10 eV, which can be related to the catalytic strength of this particle. Two bottom lines of the table show the data computed for two isomers of $Fe_{13}C_{20}$, which are nearly degenerate in total energy. The energy of the $Fe_{13}C_{20} \rightarrow Fe_{13} + C_5 + 3C_3 + 2C_2 + 2C$ fragmentation channel is larger than that of the $Fe_{13}C_{20} \rightarrow Fe_{13} + 2C_4 + 4C_3$ channel by +13.65 eV which is nearly the same as the difference in the corresponding carbon atomization energies taken with the opposite sign. This causes the total atomization energies in column **6** to practically match each other. That is, there is a competition for a carbon atom between the binding to the iron particle with or without the formation of a C−C bond at low carbon coverage. When the binding capability of the catalyst surface is exhausted, further adding of carbon atoms should likely lead to formation of such carbon structures whose atomization energies are the largest possible ones. Our energy estimates from Table 3 can be used for obtaining parameters in different models of the CNT growth[103−105] on iron catalysts. The results of this work can be used as the starting point for investigations into the catalytic growth of graphene and CNTs on iron particles at high temperatures and pressures.

IV. SUMMARY

This work addresses the patterns in the lowest total energy distributions of carbon atoms chemisorbed on the surface of an Fe_{13} particle. This iron particle possesses a nearly icosahedral geometry that allows one to not consider the effects of the surface inhomogeneity. It is found that the energetically

dx.doi.org/10.1021/jp300403p | J. Phys. Chem. C XXXX, XXX, XXX−XXX

Table 3. Carbon Atomization Energies for the Lowest Total Energy States of $Fe_{13}C_n$ and C_n[a]

				carbon atomization energies		
n	carbon pattern	channel	channel D_o/D_e	product C_i	total	C_n[b]
1	**2**	**3**	**4**	**5**	**6**	**7**
1	1	$Fe_{13}C \rightarrow Fe_{13} + C$	6.68	0.0	6.68	
2	2	$Fe_{13}C_2 \rightarrow Fe_{13} + C_2$	7.32	6.50	13.82	6.50
3	3	$Fe_{13}C_3 \rightarrow Fe_{13} + C_3$	6.25	14.17	20.42	14.17
4	211	$Fe_{13}C_4 \rightarrow Fe_{13} + C_2 + 2C$	21.28	6.50	27.78	19.74
5	221	$Fe_{13}C_5 \rightarrow Fe_{13} + 2C_2 + C$	22.02	13.00	35.02	27.16
6	2211	$Fe_{13}C_6 \rightarrow Fe_{13} + 2C_2 + 2C$	28.88	13.00	41.88	32.94
7	22111	$Fe_{13}C_7 \rightarrow Fe_{13} + 2C_2 + 3C$	36.55	13.00	49.55	40.10
8	221111	$Fe_{13}C_8 \rightarrow Fe_{13} + 2C_2 + 4C$	43.99	13.00	56.99	46.03
9	222111	$Fe_{13}C_9 \rightarrow Fe_{13} + 3C_2 + 3C$	44.42	19.51	63.92	53.07
10	222211	$Fe_{13}C_{10} \rightarrow Fe_{13} + 4C_2 + 2C$	45.21	26.01	71.21	61.33
11	222221	$Fe_{13}C_{11} \rightarrow Fe_{13} + 5C_2 + C$	46.54	32.51	79.04	66.74
12	222222	$Fe_{13}C_{12} \rightarrow Fe_{13} + 6C_2$	46.85	39.01	85.86	73.13
13	322222	$Fe_{13}C_{13} \rightarrow Fe_{13} + C_3 + 5C_2$	45.26	46.67	91.93	80.09
14	332222	$Fe_{13}C_{14} \rightarrow Fe_{13} + 2C_3 + 4C_2$	44.49	54.34	98.83	88.43
15	333222	$Fe_{13}C_{15} \rightarrow Fe_{13} + 3C_3 + 3C_2$	43.08	62.02	105.10	93.71
16	333322	$Fe_{13}C_{16} \rightarrow Fe_{13} + 4C_3 + 2C_2$	41.55	69.69	111.24	100.17
17	333332	$Fe_{13}C_{17} \rightarrow Fe_{13} + 5C_3 + C_2$	39.94	77.36	117.30	107.13
18	333333	$Fe_{13}C_{18} \rightarrow Fe_{13} + 6C_3$	38.01	85.03	123.04	115.10
19	433333	$Fe_{13}C_{19} \rightarrow Fe_{13} + C_4 + 5C_3$	38.44	90.60	129.04	120.48
20	443333	$Fe_{13}C_{20} \rightarrow Fe_{13} + 2C_4 + 4C_3$	39.05	97.65	136.70	126.95
20	5333221	$Fe_{13}C_{20} \rightarrow Fe_{13} + C_5 + 3C_3 + 2C_2 + 2C$	52.69	84.00	136.69	

[a]All energy values are in eV. The ZPVEs are accounted for up to $n = 10$ for $Fe_{13}C_n$. [b]The $C_n \rightarrow nC$ energies. Bold numbers **1**, **2**, **3**, ..., **7** in the head are given for the reference purpose.

preferred structures correspond to formation of a C_2 dimer and a C_3 trimer in $Fe_{13}C_2$ and $Fe_{13}C_3$, respectively. The favorable carbon configuration on $Fe_{13}C_4$ consists of C_2 and two single C atoms, and the further build-up proceeds in such a way as to arrive at 6 C_2 in an octahedral configuration in $Fe_{13}C_{12}$. The lowest total energy state of $Fe_{13}C_{13}$ possesses the geometrical configuration formed by adding a C atom to a dimer in the lowest energy state of $Fe_{13}C_{12}$. The adding of carbons to the $Fe_{13}C_{12}$ dimers continues up to $n = 18$, where six trimers of $Fe_{13}C_{18}$ form an octahedral configuration around the Fe_{13} core. Adding a C atom to a trimer of $Fe_{13}C_{18}$ leads to formation of a carbon tetramer in $Fe_{13}C_{19}$; however, the trend in the tetramer formation breaks in $Fe_{13}C_{20}$, where the composition of a pentamer, three trimers, two dimers, and a single C atom is energetically preferred.

We explored the dependence of total energies on the total spin in $Fe_{13}C_8$ and Fe_{13} and found that the behavior of their total energies as a function of the total spin is nearly the same. In both cases, the ferromagnetic states are energetically preferred, and the antiferromagnetic states are higher in total energy. The spin multiplicity of $Fe_{13}C_8$ in its lowest state is 37, and it is quenched with respect to the spin multiplicity of 45 of the Fe_{13} ground state. Such a quenching to $2S + 1 = 37$ and occasionally to 35 is typical for all other lowest energy states of $Fe_{13}C_n$ for $n > 6$. The reason for this quenching is explained in terms of natural atomic orbital populations.

The abstraction energies of a single carbon atom from $Fe_{13}C_n$ and C_n are on the average close to each other. However, while the $Fe_{13}C_n \rightarrow Fe_{13}C_{n-1} + C$ energies show slow variations, the $C_n \rightarrow C_{n-1} + C$ energy curve possesses a sawtooth shape with the prominent peaks at $n = 10$, 14, and 18, which correspond to the most stable cumulene structures of the carbon rings. Among the dissociation channels $Fe_{13}C_n \rightarrow Fe_{13} + C_n$, the largest energy of ~12 eV belongs to the channel $Fe_{13}C_{12} \rightarrow Fe_{13} + C_{12}$. Comparison of atomization energies for the carbon chemisorbed on the iron particle ($Fe_{13}C_n \rightarrow Fe_{13} + \sum C_i \rightarrow Fe_{13} + nC$) and atomization energies of the ground-state C_n species ($C_n \rightarrow nC$) show that the atomization energies of carbon chemisorbed on Fe_{13} are larger by approximately 10 eV, which can be related to the catalytic strength of this particle.

■ ASSOCIATED CONTENT

Supporting Information

Tables containing the data used for the plotting of Figure 7−11 are provided. The coordinates of all optimal structures in Figures 1−6 are also included. This material is available free of charge via the Internet at http://pubs.acs.org.

■ AUTHOR INFORMATION

Corresponding Author

*E-mail: gennady.gutsev@famu.edu.

Notes

The authors declare no competing financial interest.

■ ACKNOWLEDGMENTS

This research was supported by a grant from the Defense Threat Reduction Agency (Grant No. HDTRA1-09-1-0025). The research was also supported in part by the National Science Foundation through TeraGrid resources provided by NCSA and also through EPS-1003897. Portions of this research were conducted with high performance computational resources provided by the Louisiana Optical Network Initiative (http://www.loni.org). P.J. also acknowledges partial support from the Department of Energy.

■ REFERENCES

(1) Su, M.; Zheng, B.; Liu, J. *Chem. Phys. Lett.* **2000**, *322*, 321−326.

(2) Dai, H.; Rintzler, A. G.; Nikolaev, P.; Thess, A.; Colbert, D. T.; Smalley, R. E. *Chem. Phys. Lett.* **1996**, *260*, 471−475.
(3) Nikolaev, P.; Bronikowski, M. J.; Bradley, R. K.; Rohmund, F.; Colbert, D. T.; Smith, K. A.; Smalley, R. E. *Chem. Phys. Lett.* **1999**, *313*, 91−97.
(4) Harutyunyan, A. R.; Mora, E.; Tokune, T.; Bolton, K.; Rosén, A.; Jiang, A.; Awasthi, N.; Curtarolo, S. *Appl. Phys. Lett.* **2007**, *90* (163120), 1−3.
(5) Ding, F.; Larsson, P.; Larsson, J. A.; Ahuja, R.; Duan, H.; Rosén, A.; Bolton, K. *Nano Lett.* **2008**, *8*, 463−468.
(6) Jiang, A.; Awasthi, N.; Kolmogorov, A. N.; Setyawan, W.; Börjesson, A.; Bolton, K.; Harutyunyan, A. R.; Curtarolo, S. *Phys. Rev. B* **2007**, *75* (205426), 1−10.
(7) Cui, R.; Zhang, Y.; Wang, J.; Zhou, W.; Li, Y. *J. Phys. Chem. C* **2010**, *114*, 15547−15552.
(8) Raty, J.-Y.; Gygi, F.; Galli, J. *Phys. Rev. Lett.* **2005**, *95* (096103), 1−4.
(9) Larsson, P.; Larsson, J. A.; Ahuja, R.; Ding, F.; Yakobson, B. I.; Duan, H.; Rosén, A.; Bolton, K. *Phys. Rev. B* **2007**, *75* (115419), 1−6.
(10) Harutyunyan, A. R.; Awasthi, N.; Jiang, A.; Setyawan, W.; Mora, E.; Tokune, T.; K. Bolton, K.; Curtarolo, S. *Phys. Rev. Lett.* **2008**, *100* (195502), 1−4.
(11) Irle, S.; Ohta, Y.; Okamoto, Y.; Page, A. J.; Wang, Y.; Morokuma, K. *Nano Res.* **2009**, *2*, 755−767.
(12) Page, A. J.; Yamane, H.; Ohta, Y.; Stephan Irle, S.; Morokuma, K. *J. Am. Chem. Soc.* **2010**, *132*, 15699−15707.
(13) Deng, W.-Q.; Xu, X.; Goddard, W. A. *Nano Lett.* **2004**, *4*, 2331−2335.
(14) Diéguez, O.; Alemany, M. M. G.; Rey, C.; Ordejón, P.; Gallego, L. J. *Phys. Rev. B* **2001**, *63* (205407), 1−6.
(15) Bobadova-Parvanova, P.; Jackson, K. A.; Srinivas, S.; Horoi, M.; Köhler, C.; Seifert, G. *J. Chem. Phys.* **2002**, *116*, 3576−3587.
(16) Köhler, C.; Seifert, G.; Frauenheim, T. *Chem. Phys.* **2005**, *309*, 23−31.
(17) Piotrowski, M. J.; Piquini, P.; Da Silva, J. L. F. *Phys. Rev. B* **2010**, *81* (155446), 1−14.
(18) Berski, S.; Gutsev, G. L.; Mochena, M. D.; Andrés, J. *J. Phys. Chem. A* **2004**, *108*, 6025−6031.
(19) Gutsev, G. L.; Bauschlicher, C. W. Jr.; Zhai, H.-J.; Wang, L. S. *J. Chem. Phys.* **2003**, *119*, 11135−11145.
(20) Gutsev, G. L.; Mochena, M. D.; Johnson., E.; Bauschlicher, C. W. Jr. *J. Chem. Phys.* **2006**, *125* (194312), 1−11.
(21) Gutsev, G. L.; Mochena, M. D.; Bauschlicher, C. W. Jr. *J. Phys. Chem. A* **2004**, *108*, 11409−11418.
(22) Yang, S.; Taylor, K. J.; Craycraft, M. J.; Conceicao, J.; Pettiette, C. L.; Cheshnovsky, O.; Smalley, R. E. *Chem. Phys. Lett.* **1988**, *144*, 431−436.
(23) Lépine, F.; Allouche, A. R.; Baguenard, B.; Bordas, Ch.; Aubert-Frécon, M. *J. Phys. Chem. A* **2002**, *106*, 7177−7183.
(24) Arnold, D. W.; Bradforth, S. E.; Kitsopoulos, T. N.; Neumark, D. M. *J. Chem. Phys.* **1991**, *95*, 8753−8764.
(25) Kohno, M.; Suzuki, S.; Shiromaru, H.; Moriwaki, T.; Achiba, Y. *Chem. Phys. Lett.* **1998**, *282*, 330−334.
(26) Achiba, Y.; Kohno, M.; Ohara, M.; Suzuki, S.; Shiromaru, H. *J. Electron Spectrosc. Relat. Phenom.* **2005**, *142*, 231−240.
(27) Grossman, J. C.; Mitas, L.; Raghavachari, K. *Phys. Rev. Lett.* **1995**, *75*, 3870−3873.
(28) Wang, Z.; Day, P.; Patcher, R. *Chem. Phys. Lett.* **1996**, *248*, 121−126.
(29) Bylaska, E, J.; Taylor, P. R.; Kawai, R.; Weare, J. H. *J. Phys. Chem.* **1996**, *100*, 6966−6972.
(30) Galli, G.; Gygi, F.; J Golaz, J.-C. *Phys. Rev. B* **1998**, *57*, 1860−1867.
(31) An, W.; Gao, Y.; Bulusu, S.; Zeng, X. C. *J. Chem. Phys.* **2005**, *122* (204109), 1−8.
(32) Feyereisen, M.; Gutowski, M.; Simons, J.; Almlöf, J. *J. Chem. Phys.* **1992**, *96*, 2926−2932.
(33) Steimle, T. C.; Virgo, W. L.; Hostutler, D. A. *J. Chem. Phys.* **2002**, *117*, 1511−1516.
(34) Tzeli, D.; Mavridis, A. *J. Chem. Phys.* **2003**, *118*, 4984−4986.
(35) Tzeli, D.; Mavridis, A. *J. Chem. Phys.* **2005**, *122* (056101), 1−2.
(36) Tzeli, D.; Mavridis, A. *J. Chem. Phys.* **2010**, *132* (194312), 1−4.
(37) Kulik, H. J.; Marzari, N. *J. Chem. Phys.* **2010**, *133* (114103), 1−16.
(38) Fan, J.; Wang, L. S. *J. Phys. Chem.* **1994**, *98*, 11814−11817.
(39) Arbuznikov, A. V.; Hendrickx, M.; Vanquickenborne., L. G. *Chem. Phys. Lett.* **1999**, *310*, 515−522.
(40) Rayón, V. M.; Redondo, P.; Barrientos, C.; Largo, A. *J. Phys. Chem. A* **2007**, *111*, 6345−6353.
(41) Wang, L. S.; Li, X. *J. Chem. Phys.* **2000**, *112*, 3602−3608.
(42) Cao, Z.; Zhang, Q. *Int. J. Quantum Chem.* **2003**, *93*, 275−279.
(43) Fan, J.; Lou, L.; Wang, L. S. *J. Chem. Phys.* **1995**, *102*, 2701−2707.
(44) Nash, B. K.; Rao, B. K.; Jena, P. *J. Chem. Phys.* **1996**, *105*, 11020−11024.
(45) Noya, E. G.; Longo, R. C.; Gallego, L. J. *J. Chem. Phys.* **2003**, *119*, 11130−11134.
(46) Hendrickx, M. F. A.; Clima, S. *Chem. Phys. Lett.* **2004**, *388*, 290−296.
(47) Redondo, P.; Largo, L.; Barrientos, C. *Chem. Phys.* **2009**, *364*, 1−13.
(48) Largo, L.; Barrientos, C.; Redondo, P. *J. Chem. Phys.* **2009**, *130* (134304), 1−10.
(49) Zhu, W.; Li, G. *Int. J. Mass Spectrom.* **2009**, *281*, 63−71.
(50) Noya, E. G.; Longo, R. C.; Gallego, L. J. *J. Chem. Phys.* **2004**, *120*, 2069−2070.
(51) Ryzhkov, M. V.; Ivanovskii, A. L.; Delley, B. T. *Acc. Chem. Res.* **2008**, *119*, 313−318.
(52) Ryzhkov, M. V.; Ivanovskii, A. L.; Delley, B. T. *Chem. Phys. Lett.* **2005**, *404*, 400−408.
(53) Sun, M. Y.; Yang, C. L.; Wang, M. S.; Gong, Y. B.; Zhu, Y. T.; Liu, W. *J. Phys. Chem. A* **2008**, *112*, 4556−4561.
(54) Gutsev, G. L.; Bauschlicher, C. W. Jr. *Chem. Phys.* **2003**, *291*, 27−40.
(55) Zhang, Z. X.; Cao, B. B.; Duan, H. M. *J. Mol. Struct. (Theochem)* **2008**, *863*, 22−27.
(56) Helden, G.; von; Gotts, N. G.; Maitre, P.; Bowers, M. T. *Chem. Phys. Lett.* **1994**, *227*, 601−608.
(57) Noya, E. G.; Longo, R. C.; Gallego, L. J. *J. Chem. Phys.* **2003**, *119*, 11130−11134.
(58) Pradeep, T.; Kulkami, G.; Kannan, K.; Row, T. G.; Rao, C. *J. Am. Chem. Soc.* **1992**, *114*, 2272−2273.
(59) Javan, M. B.; Tajabor, N. *J. Magn. Magn. Mater.* **2011**, *324*, 52−59.
(60) Harris, H. H.; Dance, I. G. *Polyhedron* **2007**, *26*, 250−265.
(61) Pilgrim, J. S.; Duncan, M. A. *J. Am. Chem. Soc.* **1993**, *115*, 6958−6961.
(62) Durgun, E.; Dag, S.; Bagci, V. M. K.; Gülseren, O.; Yildirim, T.; Ciraci, S. *Phys. Rev. B* **2003**, *67* (201401), R1−R4.
(63) Becke, A. D. *Phys. Rev. A* **1988**, *38*, 3098−3100.
(64) Perdew, J. P.; Wang, Y. *Phys. Rev. B* **1992**, *45*, 13244−13249.
(65) Curtiss, L. A.; McGrath, M. P.; Blaudeau, J.-P.; Davis, N. E.; Binning, R. C., Jr.; Radom, L. *J. Chem. Phys.* **1995**, *103*, 6104.
(66) Frisch, M. J.; Trucks, G. W.; Schlegel, H. B.; Scuseria, G. E.; Robb, M. A.; Cheeseman, J. R.; Montgomery, Jr., J. A.; Vreven, T.; Kudin, K. N.; et al. *Gaussian 03*, revision C.02; Gaussian, Inc.: Wallingford CT, 2004.
(67) Frisch, M. J.; Trucks, G. W.; Schlegel, H. B.; Scuseria, G. E.; Robb, M. A.; Cheeseman, J. R.; Scalmani, G.; Barone, V.; Mennucci, B.; Petersson, G. A.; Nakatsuji, et al. *Gaussian 09*, rev. A.1. ed.; Gaussian Inc.: Wallingford, CT, 2009,
(68) Tremblay, B.; Gutsev, G. L.; Manceron, L.; Andrews, L. *J. Phys. Chem. A* **2002**, *106*, 10525−10531.
(69) Gutsev, G. L.; Andrews, L.; Bauschlicher, C. W. Jr. *Theor. Chem. Acc.* **2003**, *109*, 298−308.
(70) Gutsev, G. L.; Bauschlicher, C. W. Jr. *J. Phys. Chem. A* **2003**, *107*, 4755−4767.

(71) Gutsev, G. L.; Bauschlicher, C. W. Jr. *J. Phys. Chem. A* **2003**, *107*, 7013−7023.
(72) Gutsev, G. L.; Bauschlicher, C. W. Jr. *Chem. Phys. Lett.* **2003**, *380*, 435−443.
(73) Gutsev, G. L.; Bauschlicher, C. W. Jr.; Andrews, L. *J. Chem. Phys.* **2003**, *119*, 3681−3690.
(74) Zhai, H.-J.; Wang, L. S.; Jena, P.; Gutsev, G. L.; Bauschlicher, C. W. Jr. *J. Chem. Phys.* **2004**, *120*, 8996−9007.
(75) Shulga, Y. M.; Martynenko, V. M.; Baskakov, S. A.; Trukhanenok, A. N.; Anokhin, E. M.; Maksimychev, A. V.; Khasanov, S. S.; Belay, K. G.; Weatherford, C. A.; Gutsev, G. L. *Chem. Phys. Lett.* **2009**, *483*, 115−119.
(76) Gutsev, G. L.; Belay, K. G.; Weatherford, C. A.; Vasilets, V. N.; Anokhin, E. M.; Maksimychev, A. V.; Val'ba, O. V.; Martynenko, V. M.; Baskakov, S. A.; Leskova, E. S.; Shulga, Y. M. *J. Nanosci. Nanotechnol.* **2011**, *11*, 1887−1896.
(77) Huber, K. P.; Herzberg, G. *Constants of Diatomic Molecules*; Van Nostrand-Reinhold: New York, 1979.
(78) Zhao, Y.; Truhlar, D. G. *J. Chem. Phys.* **2006**, *125* (194101), 1−18.
(79) Cramer, C. J.; Truhlar, D. G. *Phys. Chem. Chem. Phys.* **2009**, *11*, 10757−10816.
(80) Yang, K.; Zheng, J.; Zhao, Y.; Truhlar, D. G. *J. Chem. Phys.* **2010**, *132* (164117), 1−10.
(81) Watts, J. D.; Bartlett, R. J. *J. Chem. Phys.* **1992**, *97*, 3445−3457.
(82) Helden, G.; van; Palke, W. E.; Bowers, M. T. *Chem. Phys. Lett.* **1993**, *212*, 247−252.
(83) Hutter, J.; Luthi, H. P.; Diederich, F. *J. Am. Chem. Soc.* **1994**, *116*, 750−756.
(84) Plattner, D. A.; Houk, K. N. *J. Am. Chem. Soc.* **1995**, *117*, 4405−4406.
(85) Martin, J. M. L.; El-Yazal, J.; François, J.-P. *Chem. Phys. Lett.* **1995**, *242*, 570−579.
(86) Martin, J. M. L.; El-Yazal, J.; François, J.-P. *Chem. Phys. Lett.* **1996**, *252*, 9−18.
(87) Jones, R. O.; Seifert, G. *Phys. Rev. Lett.* **1997**, *79*, 443−446.
(88) Giuffreda, M. G.; Deleuze, M. S.; François, J.-P. *J. Phys. Chem. A* **1999**, *103*, 5137−5151.
(89) Jones, R. O. *J. Chem. Phys.* **1999**, *110*, 5189−5199.
(90) Saito, M.; Okamoto, Y. *Phys. Rev. B* **1999**, *60*, 8939−8942.
(91) Pan, L.; Rao, B. K.; Gupta, A. K.; Das, G. P.; Ayyub, P. *J. Chem. Phys.* **2003**, *119*, 7705−7713.
(92) Belau, L.; Wheeler, S. E.; Ticknor, B. W.; Ahmed, M.; Leone, S. R.; Allen, W. D.; Schaefer, H. F.; Duncan, M. A. *J. Am. Chem. Soc.* **2007**, *129*, 10229−10243.
(93) Arulmozhiraja, S.; Ohno, T. *J. Chem. Phys.* **2008**, *128* (114301), 1−9.
(94) Rollmann, G.; Entel, P.; Sahoo, S. *Comput. Mater. Sci.* **2006**, *35*, 275−278.
(95) Köhler, C.; Frauenheim, T.; Hourahine, B.; Seifert, G.; Sternberg, M. *J. Phys. Chem. A* **2007**, *111*, 5622−5629.
(96) Gutsev, G. L.; Mochena, M. D.; Bauschlicher, C. W. Jr. *J. Nanosci. Nanotechnol.* **2006**, *6*, 1281.
(97) Mulliken, R. S. *J. Chem. Phys.* **1955**, *23* (1833−1846), 2338−2347.
(98) Reed, A. E.; Curtiss, L. A.; Weinhold, F. *Chem. Rev.* **1988**, *88*, 899−926.
(99) Jones, N. O.; Reddy, B. V.; Rasouli, F.; Khanna, S. N. *Phys. Rev. B* **2005**, *72* (165411), 1−4.
(100) Gutsev, G. L.; Weatherford, C. A.; Pradhan, K.; Jena, P. *J. Phys. Chem. A* **2010**, *114*, 9014−9021.
(101) Hoffman, R. *Tetrahedron* **1966**, *22*, 521−538.
(102) Molek, K. S.; Anfuso-Cleary, C.; Duncan, M. A. *J. Phys. Chem. A* **2008**, *112*, 9238−9247.
(103) Scott, C. D.; Povitsky, A.; Dateo, C.; Gökçen, T.; Willis, P. A.; Smalley, R. E. *J. Nanosci. Nanotechnol.* **2003**, *3*, 63−73.
(104) Wen, J. Z.; Goldsmith, C. F.; Ashcraft, R. W.; Green, W. H. *J. Phys. Chem. C* **2007**, *111*, 5677−5688.
(105) Celnika, M.; Westa, R.; Morgana, N.; Krafta, M.; Moisala, A.; Wen, J.; Green, W.; Richter, H. *Carbon* **2008**, *46*, 422−433.